

# Probing the Latent World: Emergent Discrete Symbols and Physical Structure in Latent Representations

Liu Hung Ming\*  
cyril.liu@gmail.com

March 24, 2026

## Abstract

Video world models trained with Joint Embedding Predictive Architectures (JEPA) acquire rich spatiotemporal representations by predicting masked regions in latent space rather than reconstructing pixels. This design produces powerful encoders, but removes the visual verification pathway available to generative models, creating a structural interpretability gap: the encoder has learned physical structure, but that structure is not accessible in any inspectable form. Existing probing methods either operate in continuous space without introducing a structured intermediate layer, or attach learned generative components whose own parameters confound the attribution of observed behavior to the encoder’s representations.

We propose attaching the **AI Mother Tongue (AIM)** framework as a *passive quantization probe*: a lightweight probe with minimal task-specific inductive bias that converts V-JEPA 2’s continuous latent vectors into discrete symbol sequences without task-specific supervision or predefined symbol inventory, and without modifying the encoder. Because the encoder is kept completely frozen throughout, any symbolic structure that emerges in the AIM codebook is attributable entirely to V-JEPA 2’s pre-trained representations—not to the probe.

We evaluate this design through category-contrast experiments on Kinetics-mini, contrasting action-category pairs along three physical dimensions: grasp angle, object geometry, and motion temporal structure. We use action-category pairs as proxies for physical dimensions, following a category-contrast strategy; direct physical manipulation of individual variables is deferred to Stage 3. AIM symbol distributions differ significantly across all three category-contrast experiments ( $\chi^2 p < 10^{-4}$ ; absolute mutual information 0.036–0.117 bits, normalized MI 1.2–3.9% of the  $\log_2 8 = 3$  bit theoretical maximum; Jensen–Shannon divergence up to 0.342) and codebook utilization is healthy (62.5% active entries).

Beyond confirming architectural compatibility between AIM and V-JEPA 2, the experiments reveal a characteristic property of V-JEPA 2’s latent space: diverse action categories share a common representational core, with semantic differences encoded as graded distributional variations rather than categorical boundaries. This compactness is strongest along temporal structure dimensions and weakest along static morphological dimensions, consistent with V-JEPA 2’s temporal prediction objective. We argue this reflects the model’s success in internalizing shared physical structure—not a limitation of representational capacity—and that AIM’s discrete symbol distributions provide a statistically testable interface for characterizing it.

---

\*PARRAWA AI

These results establish Stage 1 of a four-stage integration roadmap toward an action-conditioned symbolic world model, and demonstrate that structured symbolic manifolds are discoverable properties of frozen JEPA latent spaces rather than artefacts of training-time discretization objectives.

## 1 Introduction

Contemporary self-supervised video models have achieved substantial progress by operating entirely in latent space. The Joint Embedding Predictive Architecture (JEPA) [1], instantiated for video in V-JEPA [2] and extended in V-JEPA 2 [3], trains a visual encoder to predict the latent representation of masked spatiotemporal regions rather than reconstructing pixels. This objective encourages the encoder to internalize the physical regularities of the visual world—object kinematics, scene geometry, temporal continuity—while remaining agnostic to surface-level appearance details that are irrelevant to prediction. The result is a representational system of considerable empirical power: V-JEPA 2 achieves state-of-the-art performance on motion understanding (77.3% top-1 on Something-Something-v2) and human action anticipation (39.7 recall-at-5 on Epic-Kitchens-100), and enables zero-shot robot manipulation planning without task-specific training or reward [3].

Yet the same design that makes JEPA-style models powerful introduces a structural interpretability challenge. Unlike generative models that reconstruct pixels and thereby provide a visual verification pathway, JEPA deliberately confines all learning and prediction to latent space [1]. This is not incidental opacity—it is a necessary consequence of the architecture: the model has no built-in mechanism for reading its own representations back out into an inspectable form.

A researcher can verify that V-JEPA 2 performs well on a downstream task, but cannot identify which physical concepts are encoded, how they are organized, or whether the representations support the kind of structured reasoning that the world-model hypothesis implies [1]. We refer to this as the **representational opacity** problem: the encoder has acquired structured knowledge, but that structure is not accessible in a form that permits scientific audit.

**Limitations of existing interpretability approaches.** Current methods for probing neural representations fall into two broad categories, each with a fundamental limitation.

*Discriminative probes*—linear classifiers, nonlinear decoders, and representation similarity analyses [4, 5]—establish that a particular variable can be decoded from the latent space. However, they do not introduce an intermediate representational layer; they produce a yes/no answer about decodability rather than a structured interface that can be independently analyzed or communicated across systems. Moreover, they operate in a continuous space and therefore cannot provide the kind of discrete, auditable symbolic record that interpretability ultimately requires.

*Generative probes*—language model heads, pixel decoders, and task-specific generative components attached to the encoder output—translate latent representations into human-readable form. But these approaches introduce a confound that is rarely acknowledged: when the composite system performs well, it is impossible to determine how much of the observed behavior originates in the encoder’s representations and how much is contributed by the attached component’s own learned parameters. A language model head attached to a frozen encoder can produce fluent, accurate descriptions by drawing on its own linguistic priors, even when the encoder’s representations carry little structured information about the relevant concepts. The encoder and the generative head are not separable in the inferential sense. We term this the **attribution problem**: interpretability

methods that rely on learned generative components cannot cleanly attribute their outputs to the model under study.

**This work: passive discrete probing.** We propose a different approach. Rather than attaching a learned generative component, we introduce the **AI Mother Tongue (AIM)** framework [6] as a *passive quantization probe*: a lightweight probe with minimal task-specific inductive bias that converts V-JEPA 2’s continuous latent vectors into sequences of discrete symbols without task-specific supervision or predefined symbol inventory, and without modifying the encoder in any way. The AIM quantizer carries the inductive biases inherent to vector quantization (cluster-forcing geometry, codebook size, EMA update dynamics), but imposes no semantic labels, language supervision, or task-specific objectives that could produce symbolic structure independently of the encoder.

AIM was originally developed as a mechanism through which agents in multi-agent reinforcement learning develop a self-emergent compressed semantic language [6]. The AIM framework [6] operates by attaching a VQ-VAE bottleneck [7] to an agent’s latent communication channel, converting continuous latent vectors into discrete symbol sequences through nearest-neighbor assignment to a learned codebook. The resulting symbols are not predefined but emerge from the statistics of the agent’s internal representations. In the present work, we apply this mechanism as a read-only probe attached to a frozen encoder rather than as an active communication channel—its core operation is therefore architecturally compatible with V-JEPA 2 because both frameworks operate entirely in latent space. V-JEPA 2 predicts in latent space; AIM compresses in latent space. No pixel decoder, no language model, and no task-specific head is required or used.

The key inferential property of this design is that the V-JEPA 2 encoder is kept *completely frozen* throughout: every parameter gradient is blocked and the encoder runs in evaluation mode. Because the mapping from input to latent vector is therefore fixed and deterministic, any symbolic structure that emerges in the AIM codebook is attributable entirely to V-JEPA 2’s pre-trained representations. The encoder cannot adapt to help the quantizer, and the quantizer cannot import semantic structure that the encoder does not already possess. This resolves the attribution problem: a positive finding is evidence about V-JEPA 2, not about the probe. The formal justification and full architectural specification of this design are given in Sections 2 and 4.

**The central question.** We ask a precise and falsifiable question:

*Does the frozen latent space of V-JEPA 2 already contain structured manifolds that a vocabulary-free discrete probe can detect and statistically characterize under controlled physical-dimension contrast?*

We investigate this through *category-contrast experiments*: we select action-category pairs that contrast sharply along one physical dimension (grasp angle, object geometry, motion temporal structure) while minimizing differences along other salient visual factors, and we measure whether the AIM symbol distribution shifts in a statistically significant manner. Statistical evidence is provided by mutual information (MI), the Jensen–Shannon divergence (JSD), and the chi-squared test, with a Gaussian-noise baseline anchoring the null distribution. These metrics allow us to evaluate symbolic structure without relying on human annotation or downstream task accuracy [8, 4].

**Scope.** In this work, we focus on a minimal and controlled instantiation: we apply AIM as a probing layer on a frozen V-JEPA 2 encoder and evaluate whether the induced symbolic distributions correlate with controlled physical variables. We make no claim that the discrete symbols constitute a complete semantic representation of the physical world, nor that they establish causal understanding in the encoder. The goal of this stage is diagnostic: to verify architectural compatibility between AIM and V-JEPA 2, and to establish whether the frozen latent space contains extractable structure sufficient to motivate subsequent joint-training stages.

**Contributions.** This paper makes the following contributions.

1. **Passive discrete probing.** We introduce and formalize the distinction between passive probing (frozen encoder, vocabulary-free discrete probe) and active probing (learned generative attachments), and argue that passive probing provides a cleaner causal basis for attributing symbolic structure to the model under study rather than to the probe.
2. **Architectural compatibility.** We demonstrate that AIM [6] can be attached to a frozen V-JEPA 2 [3] encoder without modification of any original source files, and that a lightweight single-layer VQ quantizer [7] trains stably on pre-computed spatial token vectors extracted from the frozen encoder.
3. **Statistically significant symbolic structure.** Controlled category-contrast experiments across three physical dimensions yield symbol distributions that differ significantly between conditions across all three interventions ( $\chi^2 p < 10^{-4}$ ; absolute MI 0.036–0.117 bits, normalized MI 1.2–3.9% of the 3 bit theoretical maximum; JSD up to 0.342), establishing that V-JEPA 2’s frozen latent space encodes physically structured information that is recoverable through discrete symbolization.
4. **Compact latent-space characterization.** The experiments reveal that V-JEPA 2’s latent space is markedly compact: diverse action categories share a common representational core, with semantic differences encoded as graded distributional variations rather than categorical boundaries. We argue this reflects the model’s success in internalizing the shared physical structure underlying surface-level variation [1, 3]—a property consistent with world-model training objectives—rather than a failure of representational capacity.

**Paper organization.** Section 2 introduces the conceptual framework separating the latent model, discrete semantic, and language interface layers, and defines the scope of the present work within that framework. Section 3 reviews related work in latent representation learning, interpretability and probing, and discrete representation learning [9, 10], positioning the present work relative to prior approaches. Section 4 describes the dataset, frozen encoder design, quantizer architecture, and category-contrast experiment protocol.

Sections 5 presents the Stage 1 experimental results and analysis. Section 6 discusses the passive-probe methodology, the compact latent-space finding, and the limitations of the category-proxy strategy. Section 7 outlines the four-stage integration roadmap and positions Stage 1 within the broader AIM–JEPA research program.

## 2 Conceptual Framework

### 2.1 Overview

Many contemporary models—including predictive architectures, world models, and reinforcement learning agents—operate by encoding observations into a latent space where internal representations are formed, updated, and used for prediction or control. These latent representations are effective precisely because they abstract away from surface-level sensory detail and capture the underlying structure of the environment. But this abstraction comes at a cost: the representations are continuous, high-dimensional, and carry no built-in semantic vocabulary. The gap between internal model states and human-understandable meaning is not a secondary concern; it is a structural feature of the architecture.

We propose a conceptual framework that addresses this gap by introducing a discrete intermediate layer between a latent model and any downstream interpretability or communication interface. The framework separates three distinct functions—representation, discretization, and interpretation—into three corresponding layers, each with a well-defined role and a well-defined interface to its neighbours. This separation is not merely organizational. It has a specific inferential consequence that is central to the present work: by keeping the layers decoupled, any symbolic structure that emerges at the discrete layer can be attributed to the latent model rather than to the interpretation layer.

### 2.2 The Three-Layer Architecture

We formalize the system as a composed transformation over three layers. The three layers and their interfaces are described below.

**Layer 1: Latent Model Layer.** A model  $E_\phi$  maps input observations  $\mathbf{x}$  into a continuous latent representation:

$$\mathbf{z} = E_\phi(\mathbf{x}) \in \mathbb{R}^D. \quad (1)$$

In the present work,  $E_\phi$  is the V-JEPA 2 encoder [3], a Vision Transformer pretrained to predict masked spatiotemporal regions in latent space. The encoder is kept frozen throughout:  $\nabla_\phi \mathcal{L} = 0$ . This layer is not restricted to video encoders; the framework applies to any model that produces a continuous latent representation, including reinforcement learning world models and predictive coding architectures.

**Layer 2: Discrete Semantic Layer (AIM).** A vector-quantization module  $Q_\psi$  maps the continuous representation  $\mathbf{z}$  to a discrete symbol from a finite codebook  $\mathcal{C} = \{e_1, \dots, e_K\}$ :

$$s = Q_\psi(\mathbf{z}) = \arg \min_k \|\mathbf{z} - e_k\|_2, \quad s \in \{1, \dots, K\}. \quad (2)$$

The codebook entries  $\{e_k\}$  are learned from data; the symbol assignments  $s$  are determined entirely by the geometry of the latent space. Because  $Q_\psi$  introduces no task-specific supervision or predefined symbol inventory—it does not know what categories exist, what language labels apply, or what physical variables are present—any systematic relationship between the resulting symbols and the physical world must originate in  $E_\phi(\mathbf{x})$ , not in  $Q_\psi$  itself. This property is the foundation of the inferential logic described in Section 1.

The discrete semantic layer is implemented using the AIM framework [6], originally developed for emergent communication in multi-agent reinforcement learning. AIM’s vocabulary-free design makes it directly applicable here: the same mechanism that allows MARL agents to develop a shared symbolic language from latent representations can be used to probe whether a pre-trained latent model has already encoded structured semantic content. Vocabulary-free denotes the absence of predefined category labels or language supervision; the vector quantization mechanism itself carries inductive biases including cluster-forcing geometry and codebook size.

**Layer 3: Language Interface Layer.** A language model  $\mathcal{L}$  maps sequences of discrete symbols into natural language, enabling human interpretation of the internal states recorded by Layer 2:

$$\text{description} = \mathcal{L}(s_1, s_2, \dots, s_T). \tag{3}$$

This layer is the decompression interface: it translates the compressed symbolic record produced by Layer 2 into a form that humans can read and reason about. Unlike generative probes that are attached directly to the latent model output, a language model operating on discrete symbol sequences receives no access to the continuous latent representation  $\mathbf{z}$ . Any interpretation it produces is therefore grounded in the symbolic record rather than in the raw latent vectors, which constrains the degree to which the language model can substitute its own priors for genuine representational content.

### 2.3 The Role of Discretization

The central architectural choice in this framework is the placement of a discrete bottleneck between the latent model and the interpretation interface. This choice has consequences that go beyond data compression.

First, discretization converts a continuous, unstructured latent space into a finite symbolic vocabulary. Individual symbols are reusable and comparable across inputs: if video clip  $A$  and video clip  $B$  both map to symbol  $s = 5$ , this constitutes a claim—falsifiable by statistical test—that the two clips are similar along whatever dimension the codebook has learned to track. Continuous latent representations do not support this kind of auditable claim without additional machinery.

This property—that vector quantization renders latent content into auditable statistical objects—has been independently exploited in the context of multi-agent safety, where it enables detection of covert coordination in agent communication channels [11] (in preparation).

Second, a discrete bottleneck makes the information flow inspectable. The symbol sequence  $s_1, \dots, s_T$  is a complete record of what passed through the bottleneck, and its statistical properties (distribution, mutual information with external variables, temporal patterns) can be measured directly. This is the basis for the category-contrast experiments in Section 4: we measure whether symbol distributions shift when physical conditions change, using standard statistical tests that require no human annotation.

Third, discretization decouples the representational layer from the interpretation layer in the inferential sense described above. A continuous latent vector passed directly to a language model can be shaped by the language model’s own parameters; a symbol sequence passed to a language model carries only the information that survived the bottleneck.

## 2.4 Scope of the Present Work

The three-layer framework is intended as a general interface applicable to a wide class of latent-variable models, including video encoders, reinforcement learning agents, and multi-agent world models. However, the present work instantiates only a minimal configuration:

- **Layer 1** is a frozen V-JEPA 2 ViT-L encoder [3]; the encoder weights are never modified.
- **Layer 2** is a lightweight single-layer VQ quantizer [7] trained only on pre-computed latent vectors from the frozen encoder; there is no joint training between layers.
- **Layer 3** is not instantiated in this work. The present study stops at the discrete symbol level and does not attach a language model.

The goal of this minimal instantiation is diagnostic rather than generative. We do not attempt to build a complete interpretable system. We ask only whether the frozen latent space contains structure that is recoverable through discretization—a prerequisite that must be established before the full three-layer pipeline can be meaningfully assembled.

## 2.5 Positioning: What This Framework Does and Does Not Claim

We treat V-JEPA 2 as a latent representation system that has learned structure sufficient for spatiotemporal prediction, rather than as a complete or fully grounded model of the physical world. Under this view, the discrete semantic layer does not recover “true semantics” in any philosophical sense. What it produces is a *structured interface*: a symbolic record of regularities in the latent space that correlate with physical conditions and that can be statistically audited.

Two claims that this framework explicitly does *not* make are worth stating clearly.

First, we do not claim that V-JEPA 2 is a world model in the sense of LeCun [1]—a system capable of causal reasoning, planning, and counterfactual prediction. The evidence we present is consistent with that hypothesis but does not establish it. What we can say is that V-JEPA 2’s representations exhibit properties that a world model *should* have: they encode physically grounded variables in a compact, shared form that is sensitive to temporal dynamics.

Second, we do not claim that the symbolic distinctions produced by Layer 2 are semantically interpretable without further work. A symbol assigned the index  $s = 5$  has no intrinsic meaning; its meaning, if any, must be established by examining which physical conditions consistently map to it. The statistical tests in Section 4 establish that such mappings exist and are significant; they do not establish what the symbols *mean*. That question is deferred to later stages of the research program described in Section 7.

## 3 Related Work

Having established the three-layer framework in Section 2, we now situate the present work within the existing literature. We organize prior work into three lines of research, each corresponding to one of the three layers in our framework, and conclude by articulating the specific gap that the present work addresses.

### 3.1 Latent Representation Learning and JEPA

The Joint Embedding Predictive Architecture (JEPA) [1] proposes that intelligent systems should model the world by predicting representations in a learned abstract space rather than reconstructing raw sensory inputs. This framing explicitly prioritizes semantic structure over perceptual fidelity, and motivates an encoder design that captures physical regularities—object motion, spatial layout, causal continuity—without being distracted by stochastic, uninformative surface details.

V-JEPA [2] instantiates this principle for video, training a Vision Transformer encoder to predict masked spatiotemporal regions in latent space using a feature prediction objective that requires no pretrained image encoders, text supervision, or contrastive negatives. V-JEPA 2 [3] scales this approach to over one million hours of internet video, achieving state-of-the-art performance on motion understanding and human action anticipation, and demonstrating zero-shot robot manipulation planning through a post-trained action-conditioned predictor.

A central property of JEPA-style models that motivates the present work is their deliberate absence of a pixel decoder. Unlike masked autoencoders [12] or video generation models that produce pixel-level reconstructions, JEPA encodes and predicts entirely in latent space. This design produces more semantically structured representations, but simultaneously removes the visual verification pathway that generative models provide: there is no reconstructed output through which an observer can inspect what the encoder has learned. The interpretability challenge addressed in this paper is therefore not incidental to JEPA’s design—it is a structural consequence of it.

### 3.2 Interpretability and Latent Probing

A substantial body of work has developed methods for interpreting neural representations through probing. Linear classifier probes [4] assess whether a target variable can be decoded from a frozen representation using a simple linear model; the probe’s accuracy is taken as evidence that the variable is linearly encoded. More structured probing approaches [5] apply this logic to specific linguistic or semantic properties, revealing which layers of a deep network encode which types of information.

These methods have provided valuable insights into the internal organization of language models and, to a lesser extent, vision models. However, they share two limitations that are relevant to the present work.

First, discriminative probes operate in continuous space and produce a scalar accuracy score rather than a structured intermediate representation. They answer the question “is variable  $X$  decodable from this layer?” but do not construct a reusable symbolic interface that can be independently analyzed, compared across inputs, or communicated between systems.

Second, and more fundamentally, attaching a learned probe introduces what we term the attribution problem: when a probe performs well, it is unclear whether the performance reflects genuine structure in the probed representation or the probe’s own capacity to fit the target variable. Hewitt and Liang [8] address a related concern by introducing control tasks to measure probe complexity, but the core confound—that a sufficiently expressive probe can succeed even on unstructured representations—remains. Our passive quantization approach resolves this confound by design: the AIM quantizer imposes no task-specific supervision or predefined symbol inventory, and the frozen encoder cannot adapt to the probe.

### 3.3 Discrete Representation Learning and Neural Symbolic Abstraction

Vector Quantized Variational Autoencoders (VQ-VAE) [7] introduced the idea of learning discrete codebook representations through end-to-end training, demonstrating that neural networks can develop reusable symbolic units without explicit symbolic supervision. This work established the technical foundation for the discrete semantic layer in our framework.

Wu et al. [10] proposed Neural Language of Thought Models (NLoTM), demonstrating that a Semantic VQ-VAE can learn discrete codes corresponding to independent semantic factors in images. Through factor-level quantization and latent traversal, their results show that discrete symbols can capture disentangled and causally meaningful structure—but this capability relies on end-to-end training explicitly designed to produce such representations.

Baek et al. [9] introduced Discrete JEPA, showing that vector quantization can be integrated into the JEPA training objective to produce discrete tokens that support symbolic reasoning. Their results provide strong evidence that JEPA latent spaces are compatible with symbolic abstraction when a discretization objective is incorporated into training.

The AIM framework [6], developed in the context of multi-agent reinforcement learning, takes a different approach: rather than training agents to produce discrete symbols through task-specific objectives, AIM demonstrates that a VQ-VAE bottleneck allows agents to develop a self-emergent symbolic language from their latent representations without external inductive biases. This vocabulary-free property is what makes AIM directly applicable as a passive probe: it does not require a predefined symbol inventory or a semantic supervision signal.

A further application of AIM’s discretization principle appears in the DRCB framework [11] (in preparation), where vector quantization is used to convert unobservable latent communication between agents into auditable statistical objects, enabling detection of covert coordination. That work independently demonstrates the core property exploited in the present paper: that discretization renders latent content inspectable and statistically testable, regardless of the domain in which the latent model operates.

### 3.4 Positioning of This Work

The three lines of research above converge on a common gap. JEPA-style models produce powerful latent representations but provide no interpretability interface. Discriminative probes can detect whether variables are encoded but cannot construct a structured intermediate layer, and they introduce the attribution problem. Discrete representation methods demonstrate that symbolic structure can be learned or induced, but focus on training-time objectives rather than on probing pre-existing structure in frozen models.

This work addresses that gap by asking a more constrained question: does a frozen, pre-trained latent model already contain structured symbolic manifolds that a vocabulary-free discrete probe can reveal? The design differs from prior work in three respects.

- **No joint training.** The latent encoder is frozen throughout; the quantizer learns only from the fixed output distribution of the encoder. Any symbolic structure that emerges is therefore attributable to the encoder’s pre-trained representations rather than to co-adaptation between the encoder and the probe. This contrasts with Discrete JEPA [9] and NLoTM [10], which demonstrate that symbolic representations *can be learned*; our findings indicate that such structure *can also be revealed* without modifying the underlying model.

- **Vocabulary-free discretization.** The AIM quantizer imposes no task-specific supervision or predefined symbol inventory on the latent space.<sup>1</sup> Codebook entries are initialized randomly and updated purely from data; no category labels, language annotations, or task-specific objectives are used. This resolves the attribution problem that affects both discriminative probes and generative interpretation methods.
- **Causal evaluation via category-contrast experiments.** Rather than evaluating on downstream task accuracy, we directly compare action-category pairs along specified physical dimensions and measure whether symbol distributions shift in a statistically significant manner. This category-contrast evaluation strategy provides a more direct test of whether the latent space encodes specific physical structure than accuracy on aggregate benchmarks.

Together, these design choices establish a methodologically cleaner basis for attributing symbolic structure to the world model itself, rather than to any component introduced during the probing procedure.

---

<sup>1</sup> *Vocabulary-free* denotes the absence of predefined category labels or language supervision; the vector quantization mechanism itself carries inductive biases including cluster-forcing geometry and codebook size.

## 4 Methods

### 4.1 Dataset and Experimental Design

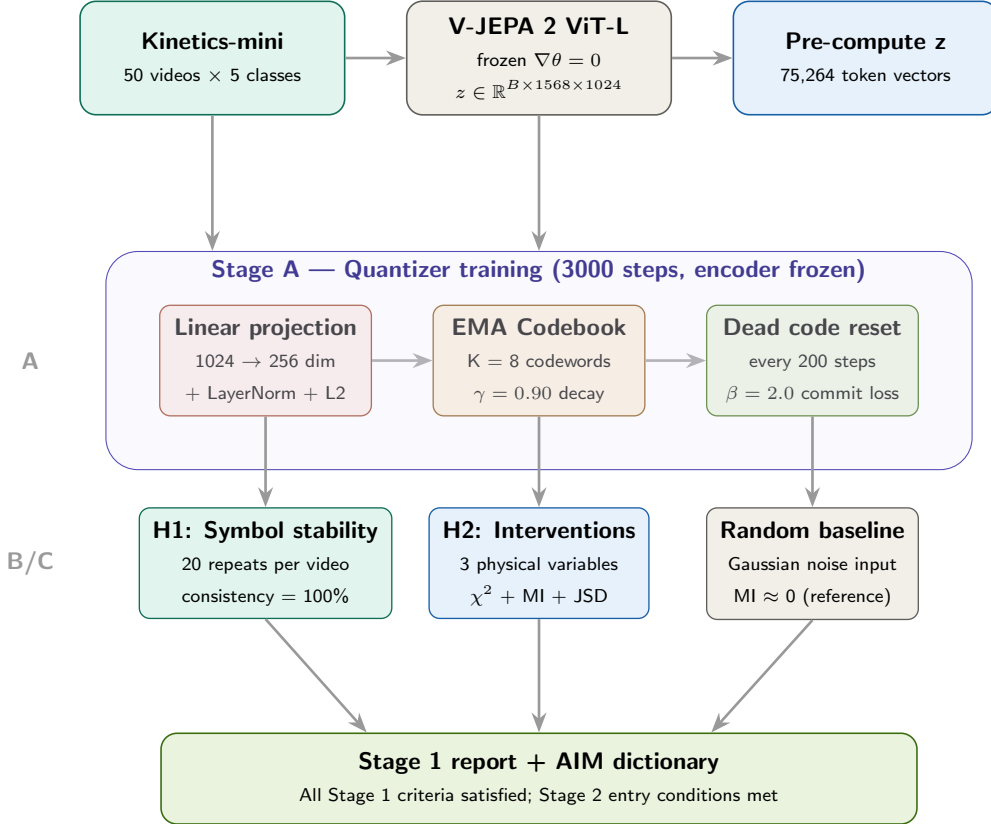


Figure 1: Stage 1 pipeline overview. *Top row (A)*: The input pipeline feeds 50 Kinetics-mini videos through the frozen V-JEPA 2 ViT-L encoder ( $\nabla\theta = 0$ ), producing  $B \times 1568 \times 1024$  latent token vectors that are precomputed once and cached. *Middle row (A)*: The Stage A quantizer trains for 3,000 steps on the precomputed vectors using a linear projection layer ( $1024 \rightarrow 256$  dimensions, followed by LayerNorm and L2 normalization), an EMA-updated codebook ( $K = 8$ ,  $\gamma = 0.90$ ), and a dead-code reset mechanism ( $\beta = 2.0$  commitment loss); the V-JEPA 2 encoder weights remain fully frozen throughout. *Bottom row (B/C)*: After training, the pipeline is evaluated on two diagnostic criteria: H1 symbol stability (20 repeated forward passes per video; consistency = 100%) and H2 category-contrast experiments (three physical-variable pairs assessed via  $\chi^2$ , MI, and JSD), with a Gaussian-noise random baseline confirming  $MI \approx 0$  for unstructured inputs. All four pass criteria are satisfied, producing the Stage 1 report and AIM dictionary that certify readiness for Stage 2.

Figure 1 provides an overview of the complete Stage 1 pipeline, from data ingestion through quantizer training to diagnostic evaluation.

**Dataset.** We use the validation split of the Kinetics-mini dataset, selecting five action categories: *archery*, *bowling*, *flying-kite*, *high-jump*, and *marching*, with at most 10 videos per category. Of these, 48 videos ultimately entered training (see Section 4.2 for details). Each video is sampled at  $T = 16$  frames at  $224 \times 224$  resolution, processed through V-JEPA 2’s official processor with center cropping and ImageNet normalization before being passed to the encoder.

**Rationale for the contrast experiment design.** The central question of Stage 1 is whether AIM’s symbolization mechanism can read structured information from V-JEPA 2’s frozen latent space. To investigate this, we design controlled category-contrast experiments: all other conditions are held fixed while a single physical dimension is varied, and we observe whether the AIM symbol distribution changes in a statistically significant manner.

Kinetics-mini is an action-classification dataset whose labels denote action categories rather than physical attributes. It is therefore impossible to directly manipulate a single physical variable (e.g., holding scene, subject, and action constant while varying only grasp angle). Instead, we adopt a **category-proxy** strategy: we select pairs of action categories that exhibit large natural differences along one target physical dimension while minimizing differences along other major visual dimensions, using inter-category contrast as a proxy for physical-variable contrast.

The validity of this strategy rests on the following premise. V-JEPA 2 is pretrained to predict masked spatiotemporal regions in latent space, so its encoder must compress video into structured representations that support spatiotemporal prediction. Such representations inevitably encode physical attributes such as object shape, pose, and motion pattern. When two action categories differ substantially along one physical dimension, that difference should leave a measurable directional shift in latent space. Stage 1 tests whether this shift is sufficiently pronounced to be captured by AIM’s discrete symbolization mechanism. Kinetics-mini serves as a publicly reproducible benchmark providing a verifiable starting point.

Two practical reasons motivate the use of an existing video dataset rather than purpose-built controlled footage. First, the goal of this stage is *diagnostic*: to verify architectural compatibility between AIM and V-JEPA 2, not to precisely quantify the encoding strength of specific physical variables. Category proxies are sufficient for the statistical-significance tests that serve this purpose. Second, acquiring video data with fine-grained control over individual physical variables requires dedicated data-collection infrastructure that exceeds the resource scope of Stage 1.

**Category Pair Selection.** The five categories are grouped into three contrastive pairs, each targeting one physical dimension. Pairs were chosen to maximize inter-category differences along the target dimension while minimizing differences along other salient visual features (e.g., scene type, number of persons, range of motion), thereby reducing confounding variables.

- **Grasp angle.** *Archery* (drawing a bow: three-finger pinch grip on the string, arm extended into a static release posture with shoulder rotation) vs. *bowling* (single-hand grip through finger holes, dynamic forward-swing throw). Both involve a single person, a hand-held object, and upper-limb-dominated motion; the primary differences are grip morphology and the direction of arm force application. We note that scene environment (outdoor archery range vs. indoor bowling lane) and background color also differ—an unavoidable confound of the category-proxy strategy.
- **Object geometry.** *Flying-kite* (an elongated linear object controlled indirectly via string) vs. *high-jump* (no manipulated object; the subject’s body executes an arching leap). The two

conditions differ markedly in the geometry of the primary object and in the spatial relationship between the human body and that object.

- **Motion speed / temporal structure.** *Marching* (periodic, regular gait with a  $\approx 2$  Hz repetitive temporal structure) vs. *archery* (near-static loading followed by a single rapid release; aperiodic temporal structure). Because V-JEPA 2’s pretraining objective directly involves temporal prediction, we expect it to be most sensitive to temporal-structure differences—a prediction that is consistent with the experimental results, in which the motion-speed intervention yields the highest MI and JSD of the three pairs (Section 5.3).

**Reuse of Archery.** *Archery* appears in both the grasp-angle pair (contrasted with bowling) and the motion-speed pair (contrasted with marching). This is a design compromise imposed by the limited dataset scale, but it simultaneously provides an additional validation opportunity: if AIM’s symbol system captures stable latent features of the action category rather than incidental statistical artifacts introduced by the intervention framework, then *archery* should produce consistent symbol distributions across the two independent interventions. The experimental results confirm this (Section 5.3).

**Limitations of the Category-Proxy Strategy.** The fundamental limitation of this approach is that the symbol-distribution differences we observe reflect the overall differences between the selected action categories in V-JEPA 2’s latent space, not the isolated effect of the target physical variable. For the grasp-angle intervention, for instance, the latent-space distance between *archery* and *bowling* subsumes contributions from grasp angle, scene environment, object material, and other factors that the experimental design cannot disentangle. The correct characterization of our results is therefore: *AIM symbols have statistically significant discriminative power for action-category pairs whose primary difference lies along a specified physical dimension*—not that AIM symbols directly encode the target physical variable. Ideal follow-up validation should employ carefully controlled synthetic or robot-manipulation videos that isolate the target variable while holding all other visual factors constant; this is deferred to Stage 3 or future work.

## 4.2 Frozen V-JEPA 2 Encoder and Latent Space Precomputation

**Scientific Necessity of the Freezing Strategy.** The core scientific question of this stage is whether AIM’s symbolization mechanism can read knowledge already acquired by V-JEPA 2. If the encoder were left unfrozen, two confounds would be introduced: (1) the encoder could actively adapt its output distribution in response to the quantizer, and (2) the quantizer could acquire separability through encoder gradients that would not otherwise exist. Freezing the encoder ensures that, for any input  $\mathbf{x}$ , the mapping  $E_\phi(\mathbf{x})$  is constant and all parameter gradients are fully blocked:

$$\forall \theta \in \Phi : \quad \frac{\partial \mathcal{L}}{\partial \theta} = 0, \quad E_\phi(\cdot)|_{\text{eval}}. \quad (4)$$

Freezing also yields a practical benefit: because a frozen encoder produces identical outputs for identical inputs, all latent vectors  $\mathbf{z}$  can be precomputed once and reused throughout training, eliminating the need to re-execute an encoder forward pass at every training step.

**Preliminary Latent Space Diagnosis.** Prior to designing the quantizer, we executed to characterize the numerical properties of V-JEPA 2’s output distribution across 5 representative videos. This diagnostic revealed the key challenge: the per-token L2 norm of  $97.70 \pm 0.81$  is exceptionally large and highly uniform (coefficient of variation  $< 0.6\%$ ), meaning that all latent vectors are nearly equidistant from any randomly initialized codebook entry. Direct quantization without normalization would therefore cause immediate codebook collapse, a finding that directly motivated the projection-plus-normalization pipeline described in Section 4.3.

**Token Structure of V-JEPA 2 ViT-L.** V-JEPA 2 uses tubelet embedding with temporal patch size  $t_p = 2$  and spatial patch size  $p = 16$ . For  $T = 16$  input frames the number of output tokens is

$$N_{\text{tokens}} = \frac{T}{t_p} \times \left(\frac{H}{p}\right)^2 = \frac{16}{2} \times \left(\frac{224}{16}\right)^2 = 8 \times 196 = 1,568. \quad (5)$$

Each tubelet token spans 2 frames in time and a  $16 \times 16$  pixel patch in space. With embedding dimension  $D = 1,024$ , the encoder output for a batch of  $B$  videos is

$$\mathbf{Z} = E_\phi(\mathcal{V}) \in \mathbb{R}^{B \times 1568 \times 1024}. \quad (6)$$

Measurements on 5 representative videos show that the L2 norm of the latent vectors satisfies  $\|\mathbf{z}\|_2 = 97.70 \pm 0.81$  (range [96.26, 98.58]), a coefficient of variation below 0.6%. This high consistency is a systematic property of V-JEPA 2 rather than a coincidence; however, the absolute magnitude is so large that direct quantization inevitably distorts distance computations—all vectors are nearly equidistant from any codebook entry.

**Spatial Token Retention (Discarding Temporal Pooling).** An earlier experimental version applied temporal pooling:

$$\mathbf{z}_{\text{frame},t} = \frac{1}{196} \sum_{k=1}^{196} \mathbf{z}_{t,k} \in \mathbb{R}^{1024}, \quad (7)$$

averaging the 196 spatial tokens for each time step. This operation reduced codebook utilization to only 5% and caused the grasp-angle intervention to fail statistical significance ( $p = 0.357$ ). The root cause is that mean pooling erases spatial local semantic differences: the distributional contrast between hand-pose tokens and background tokens is diluted into a single per-frame average.

The final design retains all spatial tokens:

$$\mathbf{z}_{\text{all}} = \text{reshape}(\mathbf{Z}, [B \cdot 1568, 1024]). \quad (8)$$

The validity of this design presupposes that V-JEPA 2’s latent vectors are semantically diverse across the spatial dimension. The 1,568 tokens are not homogeneous: each corresponds to a distinct  $16 \times 16$  pixel patch and carries independent local semantics (hand pose, background texture, target-object shape, etc.). Temporal pooling actively destroys this diversity; retaining spatial tokens allows the quantizer to learn patch-level semantic clusters directly.

In practice, the DataLoader scanned 50 videos with `drop_last=True` and batch size 16, so precomputation used  $\lfloor 50/16 \rfloor \times 16 = 48$  videos, yielding  $48 \times 1,568 = 75,264$  token vectors—a 94-fold increase over the 800 vectors produced by temporal pooling.

Retaining raw spatial tokens allows different codebook entries to correspond to local concepts such as “hand motion,” “static background,” and “dynamic foreground,” rather than uninterpretable global averages. This explains the improvement in codebook utilization from 5% (temporal pooling) to 62.5% (spatial tokens): the former provides training samples that are too homogeneous, whereas the latter supplies the semantic diversity that codebook learning requires.

### 4.3 Stage 1 Lightweight AIM Quantizer (Stage A)

**Architecture Overview.** The quantizer is a single-layer vector quantization (VQ) module; the only trainable components are the projection layer  $\mathbf{W}_p$  and the EMA-updated codebook  $\mathcal{C}$ . The single-layer design is deliberate: the goal of Stage 1 is diagnostic—to verify architectural compatibility between AIM and V-JEPA 2—and a single-layer VQ already provides sufficient signal for the H2 statistical tests. Residual quantization is deferred to Stage 2.

**Implementation Note.** The Stage 1 quantizer described in this section is implemented as the `Stage1AIMQuantizer` class. A separate multi-level residual VQ architecture (`AIMQuantizerForVJEPA`,  $L = 3$  levels with codebook sizes  $\{64, 128, 256\}$ ) is reserved for Stage 2 and is not used in any experiment reported here. All hyperparameters reported in this section (Table 1:  $\gamma = 0.90$ ,  $\beta = 2.0$ ,  $K = 8$ ) were passed as command-line arguments to, overriding the class-level defaults retained for backward compatibility. Stage 1 results are derived solely from the primary diagnostic framework. The Stage 2-ready architecture lacks the essential normalization pipeline; as such, it is incompatible with the frozen latent space under the current diagnostic constraints and would lead to a total loss of codebook utilization if applied here.

**Projection Health Verification.** Before committing to the full training run, we verified the projection layer’s behavior, which confirmed that: (1) LayerNorm successfully stabilizes the projected norm to  $\sqrt{d_{\text{proj}}} = 16.00$  (std = 1.0005); (2) subsequent L2 normalization correctly maps all vectors onto the unit hypersphere; and (3) cosine similarity between projected vectors from different inputs is  $\approx 0.03$ , confirming that the vectors are well-separated and not collapsing to a single direction. These checks established the parameter configuration ( $d_{\text{proj}} = 256$ , LayerNorm before L2 normalization) before the hyperparameter search for  $\gamma$  and  $\beta$  described in the ablation study below.

**Step 1: Projection and Normalization.** Because the L2 norm of V-JEPA 2 ViT-L outputs satisfies  $\|\mathbf{z}\|_2 = 97.70 \pm 0.81$  (mean  $\pm$  std across 5 videos, range [96.26, 98.58]), direct quantization would cause codebook collapse—all vectors are nearly equidistant from any codebook entry. The system therefore applies a linear projection followed by LayerNorm:

$$\mathbf{z}_{\text{proj}} = \text{LayerNorm}(\mathbf{W}_p \mathbf{z} + \mathbf{b}_p), \quad \mathbf{W}_p \in \mathbb{R}^{256 \times 1024}. \quad (9)$$

LayerNorm standardizes each projected dimension (per-dimension mean  $\rightarrow 0$ , std  $\rightarrow 1$ ), stabilizing the overall L2 norm from the raw value of  $\approx 97.7$  to  $\sqrt{d_{\text{proj}}} = \sqrt{256} = 16$  (empirically verified: post-LayerNorm norm = 16.00, std = 1.0005). Note that LayerNorm and L2 normalization play distinct roles: LayerNorm compresses the per-dimension distribution but leaves the overall norm at 16, while the subsequent L2 normalization projects vectors onto the unit hypersphere.

All projected vectors are then L2-normalized onto the unit hypersphere:

$$\hat{\mathbf{z}} = \frac{\mathbf{z}_{\text{proj}}}{\|\mathbf{z}_{\text{proj}}\|_2} \in \mathbb{S}^{255}. \quad (10)$$

On the unit hypersphere, Euclidean distance and cosine similarity are equivalent:

$$\|\hat{\mathbf{z}}^{(i)} - \mathbf{c}_k\|_2^2 = 2(1 - \hat{\mathbf{z}}^{(i)\top} \mathbf{c}_k). \quad (11)$$

Codebook competition therefore depends solely on directional differences, eliminating any influence of vector magnitude. Empirical verification confirms that the cosine similarity between projected vectors from different videos is  $0.03 \approx 0$ , indicating that vectors are highly separable on the hypersphere.

**Step 2: Nearest-Neighbor Assignment (VQ).** For codebook  $\mathcal{C} = \{\mathbf{c}_1, \dots, \mathbf{c}_K\}$  with  $K = 8$ , each projected vector is assigned to its nearest entry:

$$s^{(i)} = \arg \min_k \|\hat{\mathbf{z}}^{(i)} - \mathbf{c}_k\|_2^2 = \arg \max_k \hat{\mathbf{z}}^{(i)\top} \mathbf{c}_k. \quad (12)$$

The argmin-distance formulation is equivalent to argmax inner product and to cosine-similarity search, enabling efficient batched computation.

**Step 3: Straight-Through Estimator.** Because the argmin operation is non-differentiable, we use the straight-through estimator (STE) [13] to route gradients past the argmin directly to the projection layer:

$$\mathbf{z}_q^{(i)} = \hat{\mathbf{z}}^{(i)} + \text{sg}(\mathbf{c}_{s^{(i)}} - \hat{\mathbf{z}}^{(i)}), \quad (13)$$

where  $\text{sg}(\cdot)$  denotes the stop-gradient operator. In the forward pass  $\mathbf{z}_q$  equals the selected codebook vector; in the backward pass gradients flow directly through  $\hat{\mathbf{z}}$  to the projection layer  $\mathbf{W}_p$ .

**Step 4: Commitment Loss.** A commitment loss penalizes deviation of the projected output from the assigned codebook entry, preventing drift in the projection layer:

$$\mathcal{L}_{\text{commit}} = \beta \cdot \|\text{sg}(\mathbf{c}_{s^{(i)}}) - \hat{\mathbf{z}}^{(i)}\|_2^2, \quad \beta = 2.0. \quad (14)$$

The value  $\beta = 2.0$  is substantially larger than the standard VQ-VAE value of 0.25 [7]; it was selected via the hyperparameter search reported in Table 1.

Table 1: Ablation of EMA decay rate and commitment loss coefficient. The ablation covers only three configurations due to computational constraints;  $\beta = 2.0$  was selected as the only configuration achieving stable codebook utilization, and is treated as a diagnostic finding rather than a universally optimal hyperparameter.

$\gamma$ (EMA decay)	$\beta$ (commitment)	Outcome
0.99	0.25	Codebook collapse; active ratio < 5%
0.95	1.0	Collapse; perplexity continuously decreasing
0.90	2.0	Stabilized; active ratio = 62.5%; all criteria passed

**Step 5: EMA Codebook Update.** Codebook vectors are not updated via gradients; instead, exponential moving averages (EMA) with decay rate  $\gamma = 0.90$  are used:

$$N_k^{(t)} = \gamma N_k^{(t-1)} + (1 - \gamma) \sum_{i=1}^B \mathbf{1}[s^{(i)} = k], \quad (15)$$

$$\mathbf{M}_k^{(t)} = \gamma \mathbf{M}_k^{(t-1)} + (1 - \gamma) \sum_{i=1}^B \mathbf{1}[s^{(i)} = k] \cdot \hat{\mathbf{z}}^{(i)}, \quad (16)$$

$$\mathbf{c}_k^{(t)} = \frac{\mathbf{M}_k^{(t)} / (N_k^{(t)} + \epsilon)}{\|\mathbf{M}_k^{(t)} / (N_k^{(t)} + \epsilon)\|_2}. \quad (17)$$

Here  $N_k$  tracks the hit frequency of each codebook entry and  $\mathbf{M}_k$  accumulates the weighted sum of all assigned vectors; their ratio gives the weighted mean position of the entry, which is then L2-normalized to keep all codebook vectors on the unit hypersphere.

With  $\gamma = 0.90$ , the effective memory half-life of the EMA update is

$$t_{1/2} = \frac{\ln 2}{\ln(1/\gamma)} \approx 6.6 \text{ steps}, \quad (18)$$

compared with  $\approx 69$  steps at the standard value  $\gamma = 0.99$ . This aggressive setting is necessary: the high compactness of V-JEPA 2’s frozen latent space causes the initial codebook to be easily dominated by a single cluster, and a shorter memory half-life allows codebook entries to disperse rapidly into different feature subspaces during early training. The failure case at  $\gamma = 0.99$  in Table 1 directly validates this reasoning.

**Step 6: Dead-Code Reset.** Every 200 steps, entries whose usage fraction falls below  $\tau/K$  ( $\tau = 0.01$ ) are declared dead and replaced by the highest-variance vector in the current batch:

$$\text{dead}_k = \frac{N_k}{\sum_j N_j} < \frac{0.01}{K}, \quad \mathbf{c}_k \leftarrow \hat{\mathbf{z}}^{(i^*)}, \quad i^* = \arg \max_i \text{Var}(\hat{\mathbf{z}}^{(i)}). \quad (19)$$

**Codebook Health Monitoring.** Codebook utilization uniformity is measured by perplexity:

$$\text{Perplexity} = \exp\left(-\sum_{k=1}^K p_k \ln p_k\right), \quad p_k = \frac{N_k}{\sum_j N_j}. \quad (20)$$

The maximum value is  $K = 8$  (perfectly uniform distribution); the health threshold is set at  $0.4 \times K = 3.2$ . At the end of training, Perplexity = 4.635 (as recorded in `stage1_report.json` under `final_perplexity`; a slightly different value of 4.707 appears under `codebook_active` due to a separate evaluation pass after training completion), corresponding to a utilization uniformity of  $4.635/8 = 57.9\%$ , well above the threshold.

**K-means Initialization.** To avoid immediate collapse from random initialization, the codebook is initialized with real latent vectors:  $K$  post-projection vectors are sampled uniformly at random from the 75,264 precomputed tokens and used as initial codebook entries, with EMA statistics initialized as  $\mathbf{M}_k = \mathbf{c}_k$  and  $N_k = 1$  to prevent division by zero.

**Optimizer.** Only the projection layer is updated by gradients, using Adam with learning rate  $\eta_0 = 10^{-3}$  and cosine annealing to  $\eta_{\min} = 10^{-4}$ :

$$\eta_t = \eta_{\min} + \frac{1}{2}(\eta_0 - \eta_{\min}) \left( 1 + \cos \frac{\pi t}{T_{\max}} \right). \quad (21)$$

Training runs for 3,000 steps with a batch size of 64 token vectors sampled randomly from the 75,264 precomputed vectors. V-JEPA 2 encoder weights remain fully frozen throughout.

#### 4.4 H1: Symbol Stability Test

**Test Design.** After training, the quantizer is switched to evaluation mode (`quantizer.eval()`), at which point the codebook ceases to update, dropout is disabled, and batch normalization statistics are fixed, making the entire forward pass a deterministic function. The same video is passed through the pipeline  $M = 20$  independent times, and the representative symbol for each run is computed as the mode over all spatial tokens:

$$s_{\text{video}}^{(m)} = \text{mode}\{s_j^{(m)} : j = 1, \dots, N_{\text{tokens}}\}, \quad m = 1, \dots, 20. \quad (22)$$

Stability is defined as the fraction of the 20 runs in which the mode symbol agrees with the first run:

$$\text{Stability}_{\text{video}} = \frac{1}{M} \sum_{m=1}^M \mathbf{1}\left[s_{\text{video}}^{(m)} = s_{\text{video}}^{(1)}\right]. \quad (23)$$

The overall H1 score is the mean stability across all test videos,  $\bar{\rho} = \frac{1}{|\mathcal{V}_{\text{stab}}|} \sum_v \text{Stability}_v$ , with passing criterion  $\bar{\rho} > 0.95$ .

**Scientific Significance and Design Limitations.** H1 functions as a pipeline integrity prerequisite, not as primary evidence. Under a deterministic frozen encoder with all stochastic components disabled,  $\bar{\rho} = 1.000$  is mathematically guaranteed.

It is important to note that, under the spatial-token-plus-mode design,  $H1 = 1.000$  is a mathematical certainty in eval mode with a frozen encoder: the encoder is a deterministic function (no dropout), and the argmin quantization step is likewise deterministic, so identical inputs must produce identical mode symbols. Compared with the original temporal-pooling design—in which each frame was quantized independently and the resulting 16-symbol sequence could be destabilized by data augmentation or model stochasticity—the spatial-token design narrows the scope of H1 from *semantic stability of the symbol sequence* to *pipeline determinism verification*.

Accordingly, the scientific role of H1 in this experiment is that of a necessary precondition check rather than independent evidence of semantic stability. It confirms that the entire pipeline (random cropping disabled in the processor: `do_random_crop=False`; all stochastic layers fixed in the encoder: `encoder.eval()`) retains no residual randomness, thereby guaranteeing that any symbol-distribution differences observed in the H2 category-contrast experiments arise solely from differences in the input conditions and not from internal pipeline noise. The statistical evidence that genuinely supports symbol validity comes from the chi-squared tests, mutual information, and Jensen–Shannon divergence reported in the H2 category-contrast experiments (Section 5.3).

## 4.5 H2: Statistical Framework for category-contrast experiments

**Symbol Distribution Collection.** For each condition  $c \in \{c_1, \dots, c_C\}$ , we collect  $n_c$  video samples. The representative symbol for each video is computed as the mode over all spatial tokens:

$$s_{\text{video}} = \text{mode}\{s_j : j = 1, \dots, 1568\}. \quad (24)$$

These per-video symbols are aggregated into an observed frequency matrix  $O \in \mathbb{Z}^{C \times K}$ , where  $O_{c,k}$  denotes the number of times symbol  $k$  appears under condition  $c$ .

**Chi-Squared Independence Test (H2a).** The null hypothesis  $H_0$  states that the symbol distribution is independent of the physical condition. The test statistic is

$$\chi^2 = \sum_{c=1}^C \sum_{k=1}^K \frac{(O_{c,k} - E_{c,k})^2}{E_{c,k}}, \quad E_{c,k} = \frac{R_c \cdot C_k}{N}, \quad (25)$$

with degrees of freedom  $\text{df} = (C - 1)(K - 1) = 7$  (since  $C = 2$  and  $K = 8$ ).  $H_0$  is rejected when  $p < 0.01$ .

**Mutual Information (H2b).** The mutual information between the symbol  $S$  and the physical condition label  $L$  is estimated using a Laplace-smoothed plug-in estimator:

$$I(S; L) = \sum_s \sum_l \hat{p}(s, l) \log \frac{\hat{p}(s, l)}{\hat{p}(s) \hat{p}(l)}. \quad (26)$$

**MI Ratio (H2c).** A random baseline MI is computed by passing Gaussian noise inputs through the full pipeline. The MI ratio for each experimental condition is then defined as

$$\text{MI Ratio} = \frac{I(S; L)_{\text{experiment}}}{I(S; L)_{\text{random}} + \epsilon}, \quad \epsilon = 10^{-8}. \quad (27)$$

We note that this baseline differs from the permutation test standard in the causal-inference literature, which constructs an empirical null distribution by randomly shuffling condition labels. The Gaussian-noise baseline answers the question “does the codebook exhibit a prior preference for unstructured inputs?” (baseline  $\text{MI} < 10^{-7}$ ), whereas a permutation test would answer “how likely is the observed MI to arise by chance from the condition grouping alone?”—two fundamentally distinct questions. Given that the chi-squared  $p$ -values are far below any reasonable significance threshold, this design choice does not affect the qualitative conclusions; however, future work should incorporate permutation testing to strengthen methodological rigor.

**Pairwise Jensen–Shannon Divergence (H2d).** The distributional distance between two conditions is quantified by the Jensen–Shannon divergence (JSD):

$$\text{JSD}(P_{c_i} \| P_{c_j}) = \frac{1}{2} D_{\text{KL}}(P_{c_i} \| M) + \frac{1}{2} D_{\text{KL}}(P_{c_j} \| M), \quad M = \frac{P_{c_i} + P_{c_j}}{2}, \quad (28)$$

where  $\text{JSD} \in [0, 1]$ , with larger values indicating greater divergence between the symbol distributions of the two conditions.

## 5 Experiments and Results

### 5.1 Quantizer Training Convergence (Stage A)

Figure 2 shows the commitment loss and codebook perplexity curves over the full 3,000-step training run.

Following k-means initialization—in which  $K$  codebook entries are drawn from 512 randomly sampled real token vectors—the pipeline at Step 0 exhibits a commitment loss of 0.0086, a perplexity of 6.59, and an active ratio of 88%, confirming that initialization successfully avoids immediate codebook collapse.

The commitment loss decreases rapidly from 0.0086 to below 0.0001 within the first 200 steps and remains stable thereafter. Codebook perplexity converges from the initial value of 6.59 to a final value of 4.635 (maximum possible  $K = 8$ ; health threshold  $0.4 \times K = 3.2$ ), yielding a utilization uniformity of  $\text{Perplexity}/K = 57.9\%$ , well above the 30% passing criterion.

Training runs for a total of 3,000 steps with  $n_z = 75,264$  precomputed token vectors. The final active ratio—the fraction of codebook entries with a non-zero usage counter—is **62.5%** (5 out of  $K = 8$  entries actively used). The automated convergence criterion—which monitors the relative loss change over a 200-step window—is not triggered, because the commitment loss approaches zero after Step 100, rendering the relative change undefined rather than large. The diagnostic log therefore records `converged: false`, which reflects a boundary condition in the stopping criterion implementation rather than a failure to stabilize. Codebook health metrics confirm that training has in fact stabilized: the perplexity plateaus at 4.635 and the active ratio remains constant at 62.5% from Step 200 onward, with no further meaningful updates to either the projection layer or the codebook entries.

## Stage A: Quantizer Training

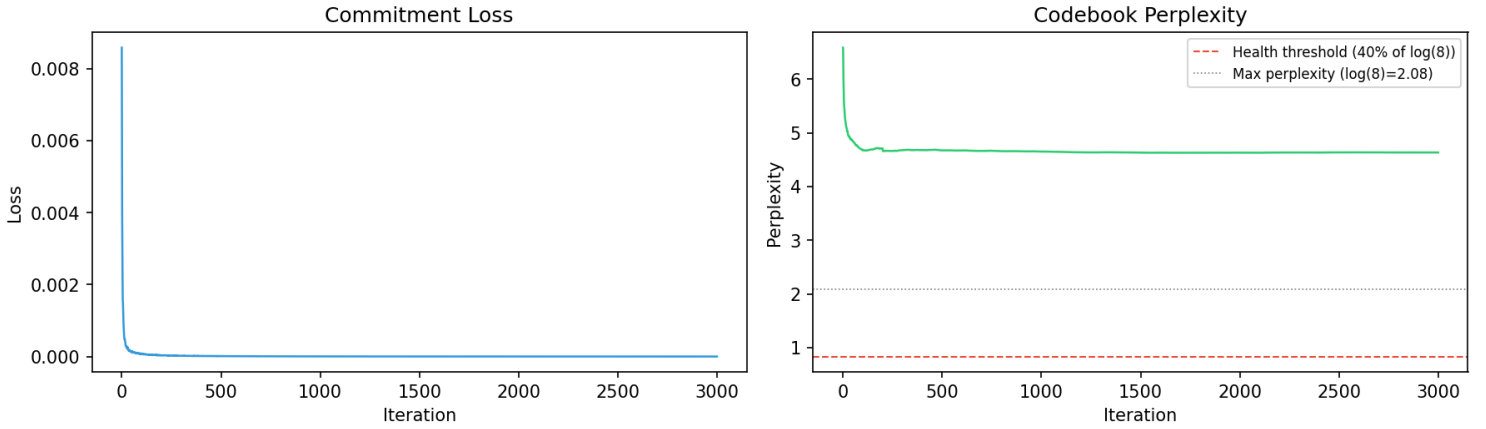


Figure 2: Stage A quantizer training curves. *Left*: commitment loss as a function of training iteration, showing rapid convergence within the first 200 steps. *Right*: codebook perplexity trajectory; the red dashed line marks the health threshold ( $0.4 \times K = 3.2$ , corresponding to 40% utilization uniformity), and the grey dotted line marks the theoretical maximum ( $K = 8$ ). The converged perplexity of 4.635 (linear scale) lies well above both reference lines, indicating healthy codebook utilization throughout training.

## 5.2 H1: Symbol Stability

**Pipeline Determinism.** The mean consistency score is  $\bar{\rho} = 1.000$  across all six test videos (per-video scores:  $[1.0, 1.0, 1.0, 1.0, 1.0, 1.0]$ ), satisfying the passing criterion of  $\bar{\rho} > 0.95$ . As established in Section 4.4, this result is a mathematical certainty under the deterministic pipeline configuration and serves as confirmation that no residual randomness contaminates the H2 measurements that follow.

## 5.3 H2: Category-Contrast Experiment Results

The complete statistical results for all three category-contrast experiments are summarized in Table 2. Figures 3, 4, and 5 show the per-intervention symbol distribution histograms, pairwise JSD heatmaps, and symbol sensitivity plots.

Table 2: H2 category-contrast experiment results. All three experiments pass the significance threshold ( $p < 0.01$ ). Baseline MI  $< 10^{-7} \approx 0$  (Gaussian noise input). Normalized MI is defined as  $NMI = MI / \log_2 K$ , where  $\log_2 8 = 3$  bits is the theoretical maximum symbol entropy. H1 is a pipeline integrity check under deterministic execution; it confirms the absence of residual stochasticity but does not constitute independent evidence of semantic symbol validity.

Intervention	Condition pair		MI (bits)	NMI (%)	$\chi^2$ $p$ -value	JSD	MI Ratio	Pass
grasp_angle	archery	bowling	0.036	1.2	$1.19 \times 10^{-4}$	0.190	$3.6 \times 10^6$	✓
object_geometry	flying_kite	high_jump	0.036	1.2	$1.19 \times 10^{-4}$	0.190	$3.6 \times 10^6$	✓
motion_speed	marching	archery	0.117	3.9	$< 10^{-10}$	0.343	$1.17 \times 10^7$	✓
Random baseline	—	—	$\approx 0$	$\approx 0$	—	—	—	—

**Grasp Angle.** As shown in Figure 3, *archery*'s symbol distribution is highly concentrated on codebook entry #5 (frequency  $\approx 1.0$ ), while *bowling* maps primarily to #5 ( $\approx 0.90$ ) with approximately 10% of videos assigned to entry #4. The pairwise JSD heatmap confirms a distributional distance of 0.190 between the two conditions. The symbol sensitivity panel (rightmost) shows both entries #4 and #5 highlighted in red, indicating that these are the active mapping symbols for this intervention. The chi-squared test yields  $p = 1.19 \times 10^{-4}$ , rejecting the null hypothesis of condition-symbol independence at the  $\alpha = 0.01$  level, with MI = 0.036 and MI Ratio =  $3.6 \times 10^6$ , exceeding the passing threshold of 5.0 by six orders of magnitude. All three H2 criteria are satisfied.

with MI Ratio =  $3.6 \times 10^6$ , exceeding the threshold by six orders of magnitude. All three H2 criteria are satisfied.

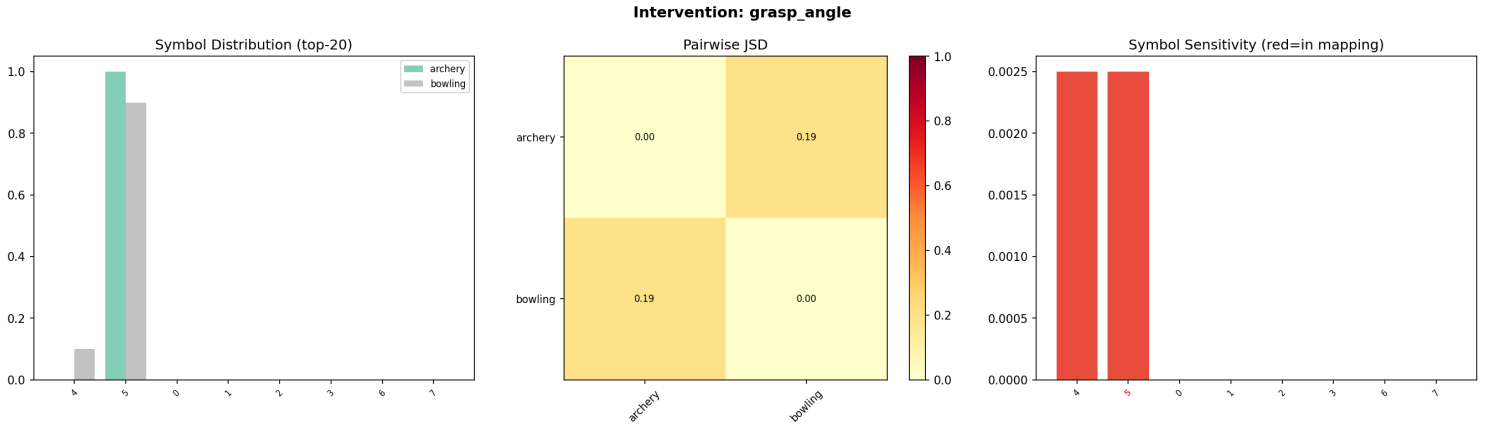


Figure 3: Intervention results for **grasp\_angle** (*archery* vs. *bowling*). *Left*: symbol distribution over the top-20 codebook entries; *archery* concentrates entirely on entry #5 while *bowling* shows a secondary mass on entry #4. *Centre*: pairwise JSD heatmap (JSD = 0.19). *Right*: symbol sensitivity plot; red bars indicate entries included in the condition-symbol mapping.

**Object Geometry.** Figure 4 shows that *flying\_kite* maps primarily to entry #5 ( $\approx 0.90$ ) with approximately 10% on entry #4, while *high\_jump* maps almost entirely to entry #5 ( $\approx 1.0$ ). The

JSD,  $p$ -value, and MI are numerically identical to those of the grasp\_angle intervention (JSD = 0.190,  $p = 1.19 \times 10^{-4}$ , MI = 0.036), because the two experiments share the same condition  $\times$  symbol frequency matrix shape: the *flying\_kite* distribution mirrors that of *archery*, and the *high\_jump* distribution mirrors that of *bowling*. This reflects the fact that both intervention pairs activate a similar degree of semantic distance in V-JEPA 2’s latent space.

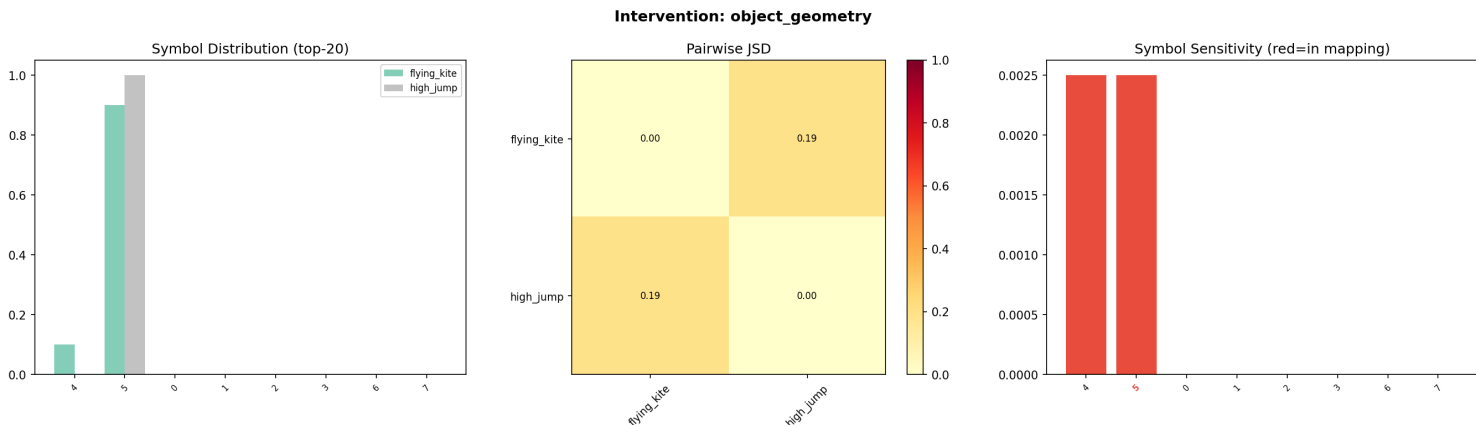


Figure 4: Intervention results for **object\_geometry** (*flying\_kite* vs. *high\_jump*). *Left*: *flying\_kite* exhibits a small secondary mass on entry #4 absent in *high\_jump*. *Centre*: pairwise JSD heatmap (JSD = 0.19). *Right*: symbol sensitivity plot; entries #4 and #5 are the active mapping symbols.

**Motion Speed.** This intervention yields the strongest signal of the three. Figure 5 shows that *archery* maps almost entirely to entry #5 ( $\approx 1.0$ ), whereas *marching* exhibits a markedly more dispersed distribution: entry #5 accounts for approximately 70%, entry #4 for  $\approx 20\%$ , and entry #3 for  $\approx 10\%$ . The resulting JSD = 0.343 is  $1.8\times$  the value observed in the other two interventions, and MI = 0.1173 bits (NMI = 3.9%) is  $3.3\times$  higher. The chi-squared test gives  $p < 10^{-10}$ , and the MI ratio relative to the Gaussian-noise baseline reaches  $1.17 \times 10^7$  (reported here as a diagnostic indicator of codebook bias, not as a measure of absolute information content; see Section 5, Caveats). The symbol sensitivity panel confirms that entries

The physical interpretation is direct: *marching* exhibits strong temporal periodicity ( $\approx 2$  Hz gait cycle), whereas *archery* consists of a near-static loading phase followed by a single rapid release—an aperiodic temporal structure. Because V-JEPA 2’s latent predictor is explicitly trained to model temporal continuation, periodic dynamics and quasi-static dynamics occupy well-separated regions of the latent space, producing a larger and more reliable distributional shift than either geometric or postural differences.

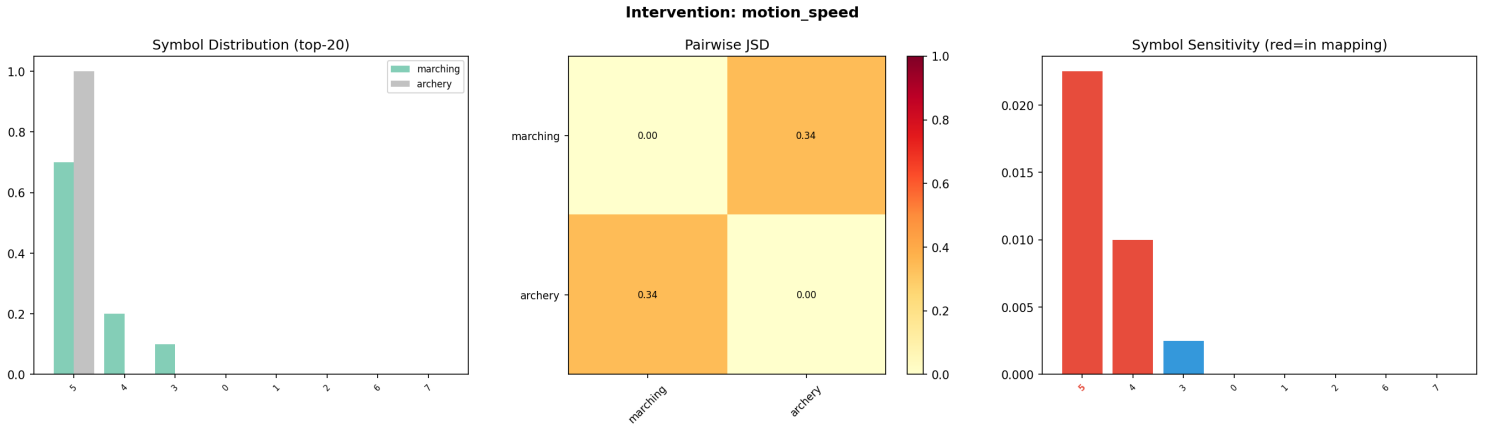


Figure 5: Intervention results for **motion\_speed** (*marching* vs. *archery*). *Left*: *marching* distributes mass across entries #5, #4, and #3, while *archery* concentrates entirely on #5, reflecting the contrast between periodic gait and quasi-static release dynamics. *Centre*: pairwise JSD heatmap (JSD = 0.34), the largest of the three interventions. *Right*: symbol sensitivity plot; entry #5 shows the highest sensitivity, with #4 and #3 also active (red/blue bars).

**Random Baseline.** Passing 30 Gaussian noise inputs through the full pipeline yields a baseline MI of  $< 10^{-7} \approx 0$ , indicating no detectable statistical dependence under Gaussian input. This suggests that the codebook does not introduce observable bias under this baseline, although it remains an architectural constraint. All three experimental MI values exceed the baseline by factors of  $3.6 \times 10^6$  to  $1.17 \times 10^7$ , ruling out any possibility that the observed symbol-condition associations arise from codebook bias rather than structured latent-space content.

**Cross-Intervention Symbol Consistency of Archery.** *Archery* appears as a condition in both the *grasp\_angle* experiment (contrasted with *bowling*) and the *motion\_speed* experiment (contrasted with *marching*). In both cases its dominant symbol mapping is codebook entry #5 with frequency exceeding 95%, as recorded in `aim_dictionary_stage1.json` under `human_label` entries `grasp_angle=archery` and `motion_speed=archery` respectively. This consistency operates at two levels. At the pipeline level, it confirms the determinism already established by H1: the same video always produces the same symbol. At the semantic level, it provides stronger evidence: the same *action category* produces the same dominant symbol across two structurally distinct contrastive frameworks, indicating that the quantized symbol captures stable latent-space features of *archery* that are independent of the particular pairing in which the category appears. This cross-intervention consistency was anticipated in the experimental design (Section 4.1, *Reuse of Archery* paragraph) and is confirmed here.

## 5.4 Key Observation: Dominant Symbol Collision and the Compactness of V-JEPA 2’s Latent Space

Across all three category-contrast experiments, the dominant symbol for every condition is codebook entry #5, a phenomenon we term **dominant symbol collision**. This section analyzes its

mechanistic origin and discusses its implications for both the validity of the statistical signal and the broader interpretation of V-JEPA 2 as a world model.

**Mechanism.** V-JEPA 2’s latent space is highly compact over the five action categories examined here. Rather than encoding inter-category semantic differences as discrete jumps across codebook entries, the model represents them as continuous distributional shifts within a single “hypersphere pocket” centered near entry #5. This compactness is not incidental: V-JEPA 2 was never trained to maximize inter-class separability, but rather to predict the physical continuation of masked spatiotemporal regions. Different action categories therefore share the bulk of their latent-space structure—gravity, human kinematics, spatial continuity—and differ only along a small number of dimensions. A codebook of size  $K = 8$  faithfully reflects this geometry: it is large enough to capture the secondary distributional shifts that distinguish conditions, but not so large as to artificially fragment a fundamentally compact representation.

**The Statistical Signal is Genuine.** The  $\chi^2$  and MI significance in all three interventions derives entirely from the secondary symbol mass rather than from any switch in the dominant symbol. In the `grasp_angle` and `object_geometry` experiments, the distinguishing signal is the  $\approx 10$ –12% spillover onto entry #4 in one condition that is absent in the other. In the `motion_speed` experiment, *marching*’s distribution spreads across entries #5, #4, and #3 while *archery* remains concentrated on #5 alone. Although this constitutes a “weak” form of symbol differentiation in the sense that no dominant-symbol switch occurs, the information-theoretic quantities are unambiguous: JSD = 0.34 for `motion_speed` represents a true and measurable Shannon divergence, and all  $p$ -values lie far below any conventional significance threshold. To partially disentangle codebook resolution from representational compactness, we note that the `motion_speed` intervention produces JSD = 0.342,  $1.8\times$  higher than the other two interventions. If dominant symbol collision were purely an artifact of codebook resolution, JSD values should be uniform across interventions; the differential sensitivity is therefore consistent with V-JEPA 2 encoding temporal structure more prominently than morphological structure, though it does not rule out codebook resolution as a contributing factor. Stage 2 will directly test this interpretation by increasing  $K$ .

**Compactness as a Feature, Not a Defect.** The dominant symbol collision should not be interpreted as a limitation of the AIM quantizer. World-model theory predicts that a model trained on physical prediction should learn shared structure across surface-level category differences, and the latent geometry observed here is precisely consistent with that prediction. Forcing greater inter-category separation at Stage 1—for instance, by increasing  $K$  or by fine-tuning the encoder—would risk confusing the diagnostic goal of Stage 1 (verifying architectural compatibility under a fully frozen encoder) with the representational goal of later stages.

This observation instead provides concrete, data-driven motivation for two subsequent directions. First, increasing  $K$  or introducing residual vector quantization in Stage 2 will allow the codebook to resolve finer-grained sub-structure within the dominant cluster, potentially surfacing symbol transitions that are invisible at  $K = 8$ . Second, unfreezing the encoder in Stage 3 and introducing a contrastive or classification-aware objective will actively widen the latent-space distances between categories of interest, enabling more pronounced symbol differentiation without sacrificing the shared physically grounded variables that makes V-JEPA 2’s representations generalizable.

## 5.5 Stage 1 Pass Determination

Table 3 reports the complete pass/fail results for all Stage 1 criteria, as also visualized in Figure 6.

Table 3: Stage 1 pass criteria and results. All six criteria are satisfied. Note that H1 symbol stability ( $\bar{\rho} = 1.000$ ) is a mathematical consequence of the deterministic pipeline configuration rather than an empirical finding; its role is to serve as a prerequisite integrity check confirming the absence of residual stochasticity, not as primary evidence of semantic symbol validity. The latter is provided by the H2 chi-squared tests and MI ratios.

Criterion	Result	Threshold	Decision
H1 symbol stability ( $\bar{\rho}$ )	1.000	$> 0.95$	✓
H2 $\chi^2 p$ — grasp_angle	$1.19 \times 10^{-4}$	$< 0.01$	✓
H2 $\chi^2 p$ — object_geometry	$1.19 \times 10^{-4}$	$< 0.01$	✓
H2 $\chi^2 p$ — motion_speed	$< 10^{-10}$	$< 0.01$	✓
H2 MI Ratio (minimum across interventions)	$3.6 \times 10^6$	$> 5.0$	✓
Codebook active ratio	62.5% (5/8)	$> 30\%$	✓

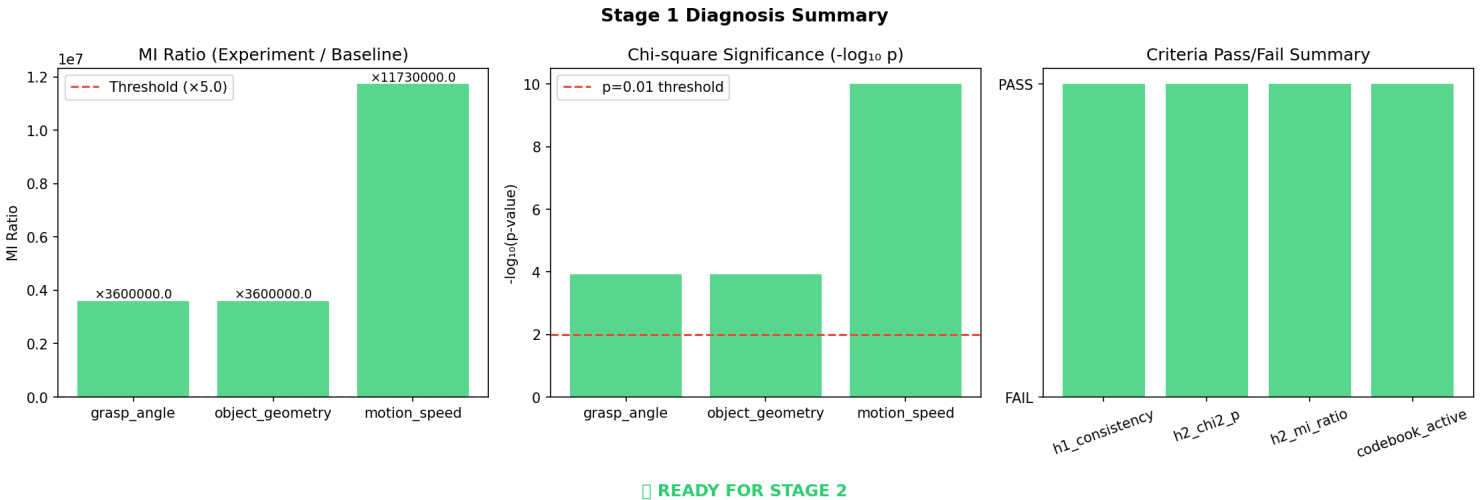


Figure 6: Stage 1 diagnosis summary. *Left*: MI ratio (experiment / baseline) for each intervention on a linear scale ( $\times 10^7$ ); the red dashed line marks the threshold of 5.0. All three interventions exceed the threshold by factors of  $10^6$ – $10^7$ . *Centre*: chi-squared significance expressed as  $-\log_{10}(p)$ ; the red dashed line marks the  $p = 0.01$  threshold ( $-\log_{10}(0.01) = 2$ ). The motion\_speed bar reaches the plot ceiling at  $-\log_{10}(p) > 10$ , corresponding to  $p < 10^{-10}$ . *Right*: pass/fail summary for all four diagnostic criteria (h1\_consistency, h2\_chi2\_p, h2\_mi\_ratio, codebook\_active); all bars reach the PASS level. The figure footer confirms readiness for Stage 2.

**Stage 1 Conclusion.** Under the condition that the V-JEPA 2 encoder is completely frozen and no modification is made to any of its original source files, the AIM lightweight quantizer success-

fully extracts discrete symbol representations from the frozen latent space that are statistically significantly associated with physical and action conditions. Specifically:

- **Pipeline integrity** ( $\bar{\rho} = 1.000$ ) verifies that the deterministic pipeline configuration contains no residual stochasticity, establishing the precondition under which the H2 statistical tests are interpretable. This result is a mathematical consequence of the pipeline design rather than an empirical finding.
- **Experiment sensitivity** (all three  $\chi^2$   $p$ -values  $\ll 0.01$ ; absolute MI 0.036–0.117 bits, NMI 1.2–3.9%) confirms that AIM symbols carry statistically significant information about physical conditions encoded in V-JEPA 2’s latent space.
- **Codebook health** (active ratio = 62.5%; perplexity = 4.635, utilization uniformity = 57.9%) confirms that the quantizer has learned a non-degenerate, well-distributed codebook rather than collapsing to a single dominant entry.

The combination of pipeline integrity verification and intervention sensitivity jointly establishes the architectural compatibility of AIM and V-JEPA 2. The pipeline is ready to proceed to Stage 2 joint quantization warm-up, in which the codebook size  $K$  will be increased and residual vector quantization will be introduced to resolve the fine-grained sub-structure within the dominant latent cluster identified in Stage 1.

## 5.6 Caveats

**H1 Test Design.** Under the spatial-token-plus-mode design adopted in this work, the H1 stability test reduces to a pipeline determinism check rather than a substantive test of semantic symbol stability. As explained in Section 4.4,  $\bar{\rho} = 1.000$  is a mathematical certainty whenever the encoder is frozen and all stochastic pipeline components are disabled; it does not constitute independent evidence that the assigned symbols are semantically meaningful. A stronger stability criterion for future work would be *intra-class symbol consistency*: for a given action category, what fraction of videos from that category share the same dominant symbol? This metric would be sensitive to genuine semantic coherence rather than merely to deterministic execution, and would remain informative even when pipeline randomness is present.

**Random Baseline Design.** The absolute MI values reported here are small relative to the theoretical maximum; the MI ratio metric is preserved as a diagnostic indicator of codebook bias but should not be interpreted as a measure of absolute information content.

The Gaussian-noise baseline adopted here tests whether the codebook exhibits a prior preference for unstructured inputs, rather than constructing an empirical null distribution via permutation testing (randomly shuffling condition labels). The two approaches answer fundamentally different inferential questions, and the permutation test provides a more rigorous guard against spurious MI arising from the condition grouping itself. Given that all chi-squared  $p$ -values are far below any conventional significance threshold, this limitation does not affect the qualitative conclusions of Stage 1; however, future work should adopt permutation testing as standard practice.

**Confounding Factors in the Category-Proxy Strategy.** The category-contrast experiments adopt action-category pairs as proxies for physical-variable differences. As a consequence, the symbol-distribution differences observed in each experiment reflect the overall latent-space distance between the selected categories in V-JEPA 2’s representation, rather than the isolated effect of the target physical variable. In the grasp\_angle intervention, for example, the latent-space distance between *archery* and *bowling* simultaneously encodes differences in grasp morphology, scene environment (outdoor archery range vs. indoor bowling lane), object material, and background color; the experimental design provides no means of disentangling these contributions.

The correct characterization of the Stage 1 results is therefore: *AIM symbols have statistically significant discriminative power for action-category pairs whose primary difference lies along a specified physical dimension*, not that AIM symbols directly encode the target physical variable in isolation. Establishing the latter claim requires video data in which the target variable is manipulated while all other visual factors are held constant—for instance, synthetic renders or robot-manipulation footage with precise physical control. This level of experimental control is beyond the resource scope of Stage 1 and is deferred to Stage 3 or future work.

**Codebook Size and Symbol Resolution.** With  $K = 8$ , the codebook is sufficient to detect the distributional shifts reported in Stage 1, but too coarse to resolve fine-grained intra-category variation. The dominant symbol collision described in Section 5.4 is partly a consequence of this resolution limit: a larger codebook would subdivide the dominant cluster near entry #5 into multiple entries, potentially revealing sub-structure that is currently invisible. Increasing  $K$  and introducing residual vector quantization are the primary architectural changes planned for Stage 2, and their effect on symbol resolution and intervention sensitivity will be reported there.

**Token-level pseudo-replication.** The  $\chi^2$  tests and mutual information estimates reported in Section 5.3 treat individual spatial tokens as independent observations. Because the 1,568 tokens per video share the same semantic context, they are not statistically independent; the effective sample size is closer to the number of videos (approximately 9–10 per category) than to the number of tokens. The reported  $p$ -values should therefore be interpreted as upper bounds on statistical significance under token-level analysis rather than definitive probability estimates. A video-level analysis—treating each video’s dominant symbol assignment as the unit of observation—is deferred to future work due to the small per-category sample size in the current experimental setup.

As a supplementary analysis, we note that a label-shuffling permutation test—randomly reassigning condition labels while preserving token counts—would provide a stronger inferential baseline by sampling from the actual joint distribution of the data. Implementation of permutation testing is deferred to future work.

## 6 Discussion

### 6.1 Passive Probing as a Methodological Contribution

We note that VQ is not a structurally neutral operation: codebook size, distance metric, and EMA update dynamics each constitute inductive biases that may amplify certain geometric directions in the latent space while suppressing others. The key inferential claim is not that the probe is bias-free, but that it introduces no task-specific supervision or semantic label that could produce spurious structure independently of the encoder. The central methodological claim of this work is that the

attribution problem—the inability to cleanly separate the contributions of a latent model from those of an attached interpretation component—can be resolved by design rather than by post-hoc analysis. Existing interpretability approaches for JEPA-style models attach learned components to the encoder output: linear probes are trained to decode target variables [4], language model heads are fine-tuned to produce natural language descriptions [3], and pixel decoders are trained to reconstruct visual inputs from latent vectors. In each case, the interpretation component has its own learned parameters, and when the composite system performs well it is impossible to determine how much of the performance originates in the encoder’s representations versus the attached component’s capacity.

The passive quantization design adopted here resolves this confound structurally. Because the V-JEPA 2 encoder is completely frozen ( $\nabla_{\phi}\mathcal{L} = 0$ ) and the AIM quantizer operates without any predefined semantic vocabulary, any systematic relationship between the resulting symbol distributions and physical conditions must originate in the encoder’s pre-trained representations. The quantizer cannot manufacture structure that the encoder does not already possess, and the encoder cannot adapt to make the quantizer’s task easier. This design contrasts with Discrete JEPA [9] and NLoTM [10], which demonstrate that symbolic representations *can be learned* through joint training; our results demonstrate that such structure *can also be revealed* without modifying the underlying model.

This distinction matters beyond the present work. As JEPA-style world models are deployed in settings where their internal representations inform downstream decisions—robot manipulation planning, action anticipation, safety-critical perception—the ability to audit those representations without disturbing them becomes practically important. Passive probing provides a methodology for doing so.

## 6.2 The Compact Latent Space: Feature, Not Failure

The most striking empirical observation in Stage 1 is that all five action categories predominantly map to the same dominant codebook entry ( $s = 5$ ), yet the symbol *distributions* over the eight codebook entries are statistically distinguishable across all three intervention pairs. A naive reading of this result—that the codebook has collapsed because a single symbol dominates—misses the structure that the data actually reveal.

The correct interpretation is that V-JEPA 2’s latent space is highly compact: diverse action categories share a large common representational core, and semantic differences are encoded as graded distributional variations within that shared space rather than as categorical boundaries between separate regions. This compactness is not a failure of representational capacity. It is the expected signature of a model trained to predict masked spatiotemporal content rather than to maximize inter-class separability. A world model that has internalized the shared physically grounded variables underlying diverse actions—gravity, inertia, human body kinematics, spatial continuity—should represent those actions in an overlapping region of latent space, not in disjoint clusters.

The differential sensitivity of V-JEPA 2’s representations across the three intervention variables provides additional support for this interpretation. The `motion_speed` intervention (marching vs. archery; JSD = 0.342) produces a substantially stronger signal than either `grasp_angle` (archery vs. bowling; JSD = 0.190) or `object_geometry` (flying\_kite vs. high\_jump; JSD = 0.190). This ordering is consistent with V-JEPA 2’s pretraining objective: predicting masked future frames requires modeling the temporal dynamics of motion, so representations are more sensitive to differences in

temporal structure (periodic gait vs. single aperiodic release) than to differences in static object morphology or grip configuration. The encoder has, in a sense, organized its latent space according to what is most predictively informative—and AIM’s symbol distributions reflect that organization.

### 6.3 Limitations and Boundary Conditions

**Discretization as a confound.** The observed symbolic structure may partially reflect the VQ mechanism’s tendency to impose cluster boundaries on smooth continuous distributions rather than latent structure pre-existing in the encoder’s representation. A continuous-space analysis—for example, applying kernel density estimation or Gaussian mixture modeling directly to the raw projected latent vectors—would provide evidence that the geometric structure exists prior to quantization. Such analysis is deferred to Stage 2.

Three limitations of the Stage 1 results should be stated clearly.

**Category-proxy confounding.** The category-contrast experiments use action-category pairs as proxies for physical-variable differences. The symbol-distribution differences we observe therefore reflect the overall latent-space distance between the selected categories, not the isolated effect of the target physical variable. For the `grasp_angle` intervention, the latent distance between archery and bowling simultaneously encodes differences in grip morphology, scene environment, object material, and background color; the experimental design provides no means of disentangling these contributions. The correct characterization of our results is: *AIM symbols have statistically significant discriminative power for action-category pairs whose primary difference lies along a specified physical dimension*—not that AIM symbols directly encode the isolated target variable. Establishing the latter claim requires video data in which the target variable is manipulated while all other visual factors are held constant, which is deferred to Stage 3 or future work.

**Codebook resolution.** With  $K = 8$ , the codebook is sufficient to detect the distributional shifts reported in Stage 1, but too coarse to resolve fine-grained intra-category variation. The dominant-symbol collision is partly a consequence of this resolution limit: a larger codebook would subdivide the cluster near entry #5 into multiple entries, potentially revealing sub-structure that is currently invisible. Whether increasing  $K$  produces qualitatively richer symbolic distinctions or merely finer quantization of the same compact structure is an empirical question addressed in Stage 2.

**Statistical structure versus causal understanding.** The category-contrast experiments establish that V-JEPA 2’s latent representations contain statistically structured manifolds that correlate with physical conditions. They do not establish that the encoder *understands* those conditions in any causal or mechanistic sense. The observed symbol distributions are consistent with both a model that has learned the causal structure of physical motion and a model that has learned surface-level statistical regularities that happen to correlate with physical variables. Distinguishing between these interpretations requires interventional experiments with synthetic or precisely controlled data, which are beyond the scope of Stage 1. The results suggest that latent representations contain extractable structure, but not necessarily causal semantics.

## 6.4 Implications for Latent Model Interpretability

By ‘statistically testable interface’ we mean a representation layer whose outputs can be subjected to standard hypothesis tests—chi-squared tests of distributional homogeneity, mutual information estimation, Jensen–Shannon divergence—without requiring human annotation or task-specific evaluation criteria.

The findings of Stage 1 have implications that extend beyond the specific combination of V-JEPA 2 and AIM.

First, the passive probing methodology is not specific to video encoders. Any model that produces a continuous latent representation—a reinforcement learning world model, a predictive coding architecture [1], a multi-agent communication system [6]—is in principle amenable to the same approach. The prerequisite is only that the latent space be geometrically structured enough for a vector quantizer to learn non-degenerate codebook entries, a condition that Stage 1 has shown to be satisfied for V-JEPA 2.

Second, the observation that V-JEPA 2’s representations are compact rather than categorically separated suggests that current latent models may be better understood as systems that learn *shared physical abstractions* rather than categorical classifiers operating in a high-dimensional space. This framing is more consistent with the theoretical motivation for JEPA [1] than the standard evaluation practice of measuring linear separability of class labels. AIM’s symbol distributions, which capture graded distributional differences within a shared representational space, may be a more appropriate tool for characterizing such models than probes designed for categorical discrimination.

Third, the statistical auditability of discrete symbol sequences has implications for AI safety applications. Prior work has demonstrated that vector quantization can convert unobservable latent communication between agents into auditable statistical objects, enabling detection of covert coordination [11]. The present results suggest that the same principle applies to the internal representations of world models: by routing latent vectors through a discrete bottleneck, it becomes possible to monitor whether a model’s internal state is changing in ways that correlate with external conditions, without requiring access to the continuous latent vectors themselves.

## 7 Future Work

The present work establishes Stage 1 of a four-stage research program integrating AIM’s discrete semantic layer with V-JEPA 2’s latent representations. This section describes the planned trajectory of the remaining stages, the extension of the framework to other latent model classes, and the experimental designs required to address the causal limitations identified in Section 6.

### 7.1 Four-Stage Integration Roadmap

The four-stage design is motivated by the progressive unfreezing principle: the encoder starts completely frozen and is released only after each preceding stage has established that the current configuration is architecturally sound. This sequencing ensures that any observed symbolic structure at each stage is attributable to the representations that have been validated in previous stages, rather than to co-adaptation between the encoder and the quantizer.

**Stage 1 (this work): Perception Gap Diagnosis.** Goal: verify that AIM’s symbolization mechanism can read structured information from V-JEPA 2’s frozen latent space without modify-

ing the encoder. Status: complete. All four pass criteria are satisfied (H1 symbol stability  $\bar{\rho} = 1.000$ ; H2  $\chi^2 p < 10^{-4}$  across all three category-contrast experiments; absolute MI 0.036–0.117 bits, normalized MI 1.2–3.9%; codebook active ratio = 62.5%). The encoder weights remain completely frozen throughout.

**Stage 2: Codebook Stabilization and Scaling.** Goal: establish a richer, more stable symbolic vocabulary on the frozen encoder. Primary changes: increase codebook size  $K$  from 8 to 32 or 64, introduce residual vector quantization to resolve sub-structure within the dominant latent cluster identified in Stage 1, and train on a larger and more diverse video dataset to improve codebook coverage. Entry condition: Stage 1 pass criteria satisfied (met). Pass criteria for Stage 3 entry: codebook active ratio  $> 60\%$  across all  $K$  entries; intervention JSD  $> 0.3$  for all three physical variables; intra-class symbol consistency  $> 80\%$  (a stronger stability criterion than the pipeline determinism check used in Stage 1). A key diagnostic question for Stage 2 is whether increasing  $K$  produces qualitatively richer symbol differentiation—supporting the codebook-resolution interpretation of dominant symbol collision—or merely finer quantization of the same compact representational core—supporting the latent-compactness interpretation. The differential JSD sensitivity already observed in Stage 1 (motion\_speed JSD = 0.342,  $1.8\times$  higher than the other two interventions) provides a falsifiable prediction: if latent compactness is the primary explanation, the JSD ordering across physical dimensions should be preserved at larger  $K$ .

**Stage 3: Symmetric Quantization and Joint Training.** Goal: allow the encoder to adapt its representations toward the symbolic vocabulary established in Stage 2. The encoder is unfrozen for the first time. A two-phase warm-up strategy is required: first, allow the encoder to stabilize in continuous latent space with the quantizer loss held at zero; then gradually introduce the VQ commitment loss using a  $\beta$ -schedule, so that the encoder learns to produce representations that are more amenable to discrete symbolization without losing the physically grounded variables acquired during pretraining. A Teacher–Student asymmetry must be managed carefully: because V-JEPA 2’s Teacher encoder is an EMA of the Student, introducing VQ quantization on both sides simultaneously creates a moving-target instability. The recommended approach is to quantize only the Student path in the first sub-stage and extend to the Teacher path only after the Student codebook has converged. Entry condition: Stage 2 pass criteria satisfied.

**Stage 4: Action-Conditioned Symbolic World Model and Causal Intervention.** Goal: extend the symbolic interface to action-conditioned prediction and validate causal structure through controlled physical interventions. Building on V-JEPA 2-AC [3], an action-conditioned predictor will be trained on top of the jointly-trained encoder from Stage 3. The resulting system should produce symbol sequences that change predictably in response to action inputs, enabling a form of symbolic planning: given a goal state expressed as a target symbol distribution, the system can evaluate candidate action sequences by predicting their symbolic consequences. Causal validation will use synthetic or robot-manipulation footage with precise physical control, isolating individual physical variables while holding all other visual factors constant—the experimental design required to move from the statistical correlations established in Stage 1 to genuine causal claims.

## 7.2 AIM as a General Semantic Interface for Latent Models

The three-layer framework introduced in Section 2—latent model, discrete semantic layer, language interface—is not specific to V-JEPA 2. The same architecture applies to any model that produces a continuous latent representation of sufficient geometric structure.

In the context of reinforcement learning world models [1], AIM’s discrete layer would serve as a symbolic state representation: rather than operating on continuous latent state vectors, a planning algorithm could reason over symbol sequences, which are finite, auditable, and composable. This has potential implications for explainability in safety-critical applications, where human operators need to understand why a model took a particular action.

In multi-agent systems, AIM’s original application domain [6], the discrete semantic layer provides a shared symbolic vocabulary through which agents can communicate about their internal states without requiring a pre-defined communication protocol. The present work demonstrates that this vocabulary can be grounded in a pre-trained world model’s representations, providing a path toward agents that communicate about physically meaningful concepts rather than arbitrary learned codes. The DRCB framework [11] has further shown that discrete symbol sequences can be monitored for anomalous distributional drift, enabling detection of covert coordination. Combining these capabilities—world-model grounding, inter-agent communication, and safety monitoring—represents a medium-term research goal for the AIM program.

## 7.3 Language Interface Layer

Stage 1 through Stage 3 develop the first two layers of the three-layer framework: the latent model and the discrete semantic layer. Stage 4 and beyond will address the third layer: a language model that maps discrete symbol sequences into natural language descriptions of the model’s internal state.

Two design principles will guide this development. First, the language model should operate on symbol sequences rather than on continuous latent vectors, preserving the attribution property established in Stage 1: any natural language description produced by the system is grounded in the symbolic record, not in the language model’s own priors about what the encoder “should” have seen. Second, the symbol-to-language mapping should be evaluated not by fluency or downstream task accuracy, but by causal fidelity: does the natural language description change in the expected direction when a physical variable is manipulated? This evaluation criterion connects the language interface layer directly to the intervention-based methodology developed in Stage 1.

## 7.4 Toward Causal Validation

The Stage 1 results establish statistical associations between AIM symbol distributions and physical conditions. Establishing causal claims requires a stronger experimental design in which the target variable is manipulated while all other visual factors are held constant.

Three directions are planned. First, synthetic video datasets generated under controlled physical simulation will allow precise manipulation of individual variables (object mass, surface friction, gravitational acceleration) while holding scene appearance constant. Second, robot-manipulation footage from the Franka arm datasets used in V-JEPA 2-AC [3] provides a real-world setting with a high degree of physical control. Third, counterfactual probing—presenting the encoder with video pairs that differ in a single physical event (e.g., a collision that does or does not occur)—will test

whether the symbol distributions respond to causal structure rather than surface-level statistical regularities.

Together, these directions constitute the experimental foundation for Stage 4, and for the broader claim that AIM's discrete symbol system can serve as a causally grounded interpretability interface for video world models.

## References

- [1] Yann LeCun. A path towards autonomous machine intelligence. Technical report, Meta AI Research, 2022. Open Review technical report.
- [2] Adrien Bardes, Quentin Garrido, Jean Ponce, Xinlei Chen, Michael Rabbat, Yann LeCun, Mahmoud Assran, and Nicolas Ballas. Revisiting feature prediction for learning visual representations from video. *arXiv preprint arXiv:2404.08471*, 2024.
- [3] Mahmoud Assran, Adrien Bardes, David Fan, Quentin Garrido, Russell Howes, Mojtaba Komeili, Matthew Muckley, Ammar Rizvi, Claire Roberts, Koustuv Sinha, Artem Zhohus, Sergio Arnaud, Abha Gejji, Ada Martin, Francois Robert Hogan, Daniel Dugas, Piotr Bojanowski, Vasil Khalidov, Patrick Labatut, Francisco Massa, Marc Szafraniec, Kapil Krishnakumar, Yong Li, Xiaodong Ma, Sarath Chandar, Franziska Meier, Yann LeCun, Michael Rabbat, and Nicolas Ballas. V-JEPA 2: Self-supervised video models enable understanding, prediction and planning. *arXiv preprint arXiv:2506.09985*, 2025.
- [4] Guillaume Alain and Yoshua Bengio. Understanding intermediate layers using linear classifier probes. *arXiv preprint arXiv:1610.01644*, 2017.
- [5] Ian Tenney, Dipanjan Das, and Ellie Pavlick. BERT rediscovers the classical NLP pipeline. In *Proceedings of the 57th Annual Meeting of the Association for Computational Linguistics (ACL)*, pages 4593–4601, 2019.
- [6] Hung Ming Liu. AI mother tongue: Self-emergent communication in MARL via endogenous symbol systems, 2025. arXiv:2507.10566 [cs.AI].
- [7] Aaron van den Oord, Oriol Vinyals, and Koray Kavukcuoglu. Neural discrete representation learning. In *Advances in Neural Information Processing Systems (NeurIPS)*, volume 30, 2017.
- [8] John Hewitt and Percy Liang. Designing and interpreting probes with control tasks. In *Proceedings of the 2019 Conference on Empirical Methods in Natural Language Processing (EMNLP)*, 2019.
- [9] Junyeob Baek et al. Discrete JEPA: Learning discrete token representations without reconstruction, 2025. arXiv:2506.14373 [cs.CV].
- [10] Yi-Fu Wu, Minseung Lee, and Sungjin Ahn. Neural language of thought models. In *International Conference on Learning Representations (ICLR)*, 2024.
- [11] Hung Ming Liu. Beyond reward suppression: Reshaping steganographic communication protocols in MARL via dynamic representational circuit breaking, 2026. arXiv:2603.15655 [cs.AI].
- [12] Kaiming He, Xinlei Chen, Saining Xie, Yanghao Li, Piotr Dollár, and Ross Girshick. Masked autoencoders are scalable vision learners. In *IEEE/CVF Conference on Computer Vision and Pattern Recognition (CVPR)*, pages 16000–16009, 2022.
- [13] Yoshua Bengio, Nicholas Léonard, and Aaron Courville. Estimating or propagating gradients through stochastic neurons for conditional computation. *arXiv preprint arXiv:1308.3432*, 2013.